NANO LETTERS

pubs.acs.org/NanoLett Letter

Engineering Electromagnetic Field Distribution and Resonance Quality Factor Using Slotted Quasi-BIC Metasurfaces

Sen Yang,[¶] Mingze He,[¶] Chuchuan Hong, Joshua D. Caldwell, and Justus C. Ndukaife*

Cite This: *Nano Lett.* 2022, 22, 8060−8067 Read Online

ACCESS | Metrics & More | Article Recommendations | Supporting Information

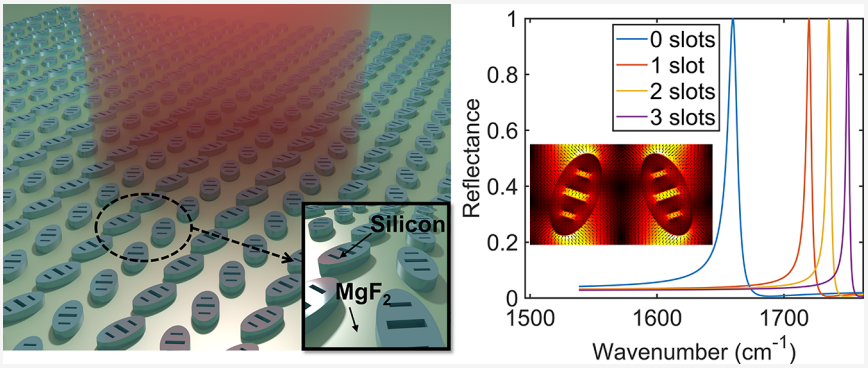

ABSTRACT: Dielectric metasurfaces governed by bound states in the continuum (BIC) are actively investigated for achieving high-quality factors and strong electromagnetic field enhancements. Traditional approaches reported for tuning the performance of quasi-BIC metasurfaces include tuning the resonator size, period, and structure symmetry. Here we propose and experimentally demonstrate an alternative approach through engineering slots within a zigzag array of elliptical silicon resonators. Through analytical theory, three-dimensional electromagnetic modeling, and infrared spectroscopy, we systematically investigate the spectral responses and field distributions of the slotted metasurface in the mid-IR. Our results show that by introducing slots, the electric field intensity enhancement near the apex and the quality factor of the quasi-BIC resonance are increased by a factor of 2.1 and 3.3, respectively, in comparison to the metasurface without slots. Furthermore, the slotted metasurface also provides extra regions of electromagnetic enhancement and confinement, which holds enormous potential in particle trapping, sensing, and emission enhancement.

KEYWORDS: *all-dielectric metasurface, bound states in the continuum, electric field enhancement, biosensing, mid-IR spectroscopy, nanoantenna*

Creation of strong electromagnetic field enhancements is essential in nanophotonics and optical devices used for many applications such as biosensing, lasing, and quantum information.[1] Plasmonic nanostructures harness the collective oscillation of conduction electrons sustained in metallic nanostructures to generate highly enhanced and tightly confined electromagnetic hotspots in the vicinity of the metallic nanostructures. However, the nonradiative absorption resulting from the intrinsic (ohmic) loss of metals naturally limits the quality factor (Q) of the resonance,[2,3] which is crucial for ultrasensitive sensing and lasing applications.[4,5] Some efforts have been made toward leveraging Fano resonances induced through interference between plasmonic resonances[6] and the collective diffractive modes in a nanoantenna array,[7] though the typical Q is still relatively low[8] (Q < 100). We note that some recent works[9,10] based on surface lattice resonances in plasmonic nanoparticle arrays reported high Qs, with a record-high of 2340,[11] although the energy dissipation is still not avoidable, which inevitably leads to photothermal heating of the plasmonic elements.[12] In parallel, to circumvent the issue of intrinsic loss in plasmonic nanostructures, high-index dielectric materials with low absorption have recently been studied as a promising alternative for light manipulation at the subwavelength scale.[13−15]

Recently, the concept of bound states in the continuum (BIC) has emerged as a powerful approach for realizing high Qs and high field enhancements in all-dielectric metasurfaces. BICs are wave solutions embedded in a radiative continuum but are completely decoupled from the radiating waves. The

Received: May 11, 2022
Revised: October 3, 2022
Published: October 10, 2022

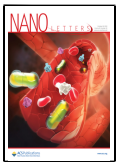

https://doi.org/10.1021/acs.nanolett.2c01919
Nano Lett. 2022, 22, 8060−8067

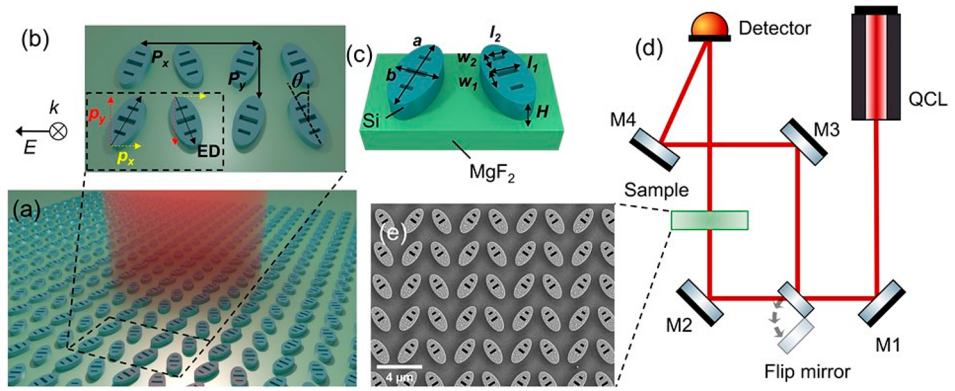

Figure 1. Design and measurements of the all-dielectric metasurface. Schematic illustration of (a) the metasurface illuminated with a collimated light beam and (b) a zoom-in view of four unit-cells of the metasurface. The metasurface comprises rectangular lattices (periods, P_x = 4247 nm, P_y = 2448 nm) of dimers formed by two slotted elliptical resonators with a tilt angle of $\theta = \pm 20°$. The region in the black dash box depicts the electric dipoles (ED) induced in the resonators. The incident light is *x*-polarized plane wave. The yellow and red dash arrows represent the two components p_x and p_y, respectively. (c) Schematic of a unit cell showing silicon elliptical resonators sitting on the magnesium fluoride (MgF_2) substrate. The geometrical parameters: a = 2124 nm, b = 1040 nm, w_1 = 600 nm, w_2 = 365 nm, l_1 = 180 nm, l_2 = 130 nm, H = 700 nm. The slot centers are aligned with the long axis of the ellipse to maintain the structure symmetry. (d) Experimental setup used for transmission laser-based spectroscopy (see the SI, section S3 for more measurement details). M1−M4, mirrors; QCL, quantum cascade laser. (e) Representative SEM image of the "2 slots" sample. The roughness of the surface results from the deposited chromium thin film, which works as a charge dissipation layer for better imaging quality.

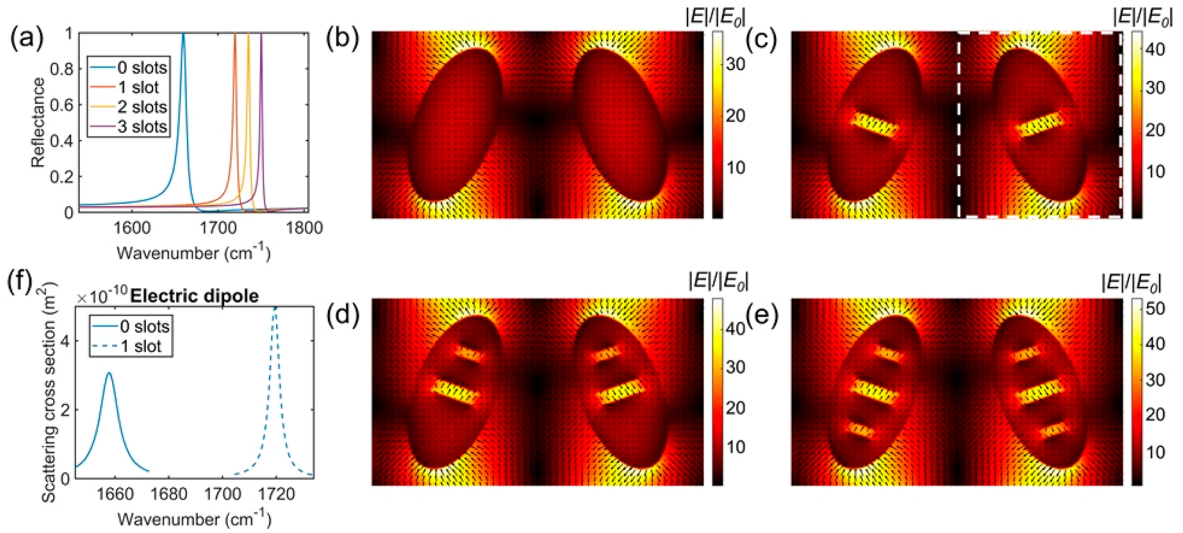

Figure 2. Optical characterization of the all-dielectric metasurface by numerical simulations. (a) Reflectance spectra of "0 slots", "1 slot", "2 slots", and "3 slots" designs. (b−e) Electric field enhancement distributions of *xy* plane at z = 350 nm for "0 slots" to "3 slots" designs, respectively. The electric field vector plot is superimposed on the field profile. Arrow length represents the magnitude of the electric field. See the SI, section S1 for simulation details. (f) Multipole decomposition analysis shows the dominant electric dipole component. The nature of the mode preserves for the slotted designs. The multipole decomposition is applied to the region enclosed by the white dashed rectangle in panel c. The solid line corresponds to the "0 slots" design while the dashed line is for the "1 slot" design. A multipole decomposition showing all multipoles are provided in the SI, section S5.

concept of BIC was first proposed in quantum mechanics by von Neumann and Eugene Wigner in 1929[16] and was then expanded to other fields of wave mechanics such as optics and acoustics.[17] BIC in optics refers to a kind of nonradiating state of light and has been demonstrated in many structures such as photonic crystals[18,19] and optical waveguides.[20] An ideal BIC has no outcoupling, making the true BIC modes inaccessible. If the outgoing radiation is minimized while not totally vanishing, a sharp peak can be observed in the spectrum with a finite Q. Such a case is called a quasi-BIC. Recently, all-dielectric metasurfaces are being investigated as a versatile tool to realize quasi-BIC in finite structures. Such low-loss platforms are highly promising for high-Q resonances comparable to photonic crystals (10^2−10^7)[21] and in some systems, the resulting strong field enhancements are comparable to or even higher than those reported in plasmonic nanostructures, providing opportunities for a variety of applications including lasing,[22−24] biosensing,[25−27] low power nano-optical trapping of particles,[28,29] and nonlinear harmonic generation.[30−33]

Currently, the mainstream method[34] of tuning the resonance of a quasi-BIC metasurface is to engineer the structure symmetry of individual resonators[35] or via parameter tuning such as modifying the dimensions of the metasurface elements to excite supercavity modes.[36,37] In this work, we propose and

https://doi.org/10.1021/acs.nanolett.2c01919
Nano Lett. 2022, 22, 8060−8067

experimentally demonstrate a new mechanism to improve the quasi-BIC resonance of an all-dielectric metasurface by introducing slots into elliptical silicon resonators arranged in a zigzag array.[25] The "normal" slot effect stems from the continuity of the normal component of the electric displacement field at high index-contrast interfaces. It has been widely leveraged to expose and enhance electromagnetic fields confined in high index materials.[38−40] In our work, besides this well-known slot effect, we demonstrate that introducing slots can also effectively increase the local electromagnetic fields close to the apexes of the constituent elliptical resonators as well as the Q of the existing quasi-BIC resonance. In addition to these, the slots also provide extra field enhancement and confinement regions due to the "normal" slot effect. Instead of introducing slots to break the symmetry and transition a true BIC to a quasi-BIC mode,[41,42] we here engineer a quasi-BIC system, and the slots are symmetrically introduced to retain the symmetry. Our slotted design therefore opens the door for designing quasi-BIC governed metasurfaces and are especially suitable for applications where high Q and multiple hotspots (i.e., electromagnetic field confined and enhanced regions) are desirable such as lasing, nonlinear optics, optical trapping, and photonic metasensors.[43]

The system we have studied is a symmetry-protected quasi-BIC-governed all-dielectric metasurface composed of elliptical silicon resonators arranged in a zigzag array. First, we symmetrically introduce 1, 2, and 3 slots into each silicon resonator (see Figure 1 and 2), respectively, and simulate their optical responses including reflectance spectra and electric field distributions. We prove that the Q and the maximum electric field intensity enhancement increase with introducing slots, up to 3.3-times and 2.1-times, respectively, when adding three slots in each resonator. Both Fourier-transform infrared (FTIR) spectroscopy and laser-based spectroscopy are carried out to cross-validate the simulated spectral responses. Next, we implement the optical nanoantenna theory to qualitatively understand the influence of slots on the spectral response. We further investigate the effects of slot geometry for the 1 slot case, which can be predicted by the optical nanoantenna theory. Moreover, our presented methodology is also readily extendable to other dipole-based resonant systems. We also note that this work is different from our prior work in ref 28, where a theoretical description of the self-induced back-action optical trapping in a quasi-BIC system was performed.

Our all-dielectric metasurface comprises slotted silicon elliptical resonators with a tilt angle arranged in a zigzag array on a magnesium fluoride (MgF_2) substrate, as shown in Figure 1a. Since one of the applications we propose is biosensing, we design our metasurface to support a resonance at 6 μm free-space wavelength near the frequencies of the amide I and II vibrational bands for proteins. Three slots are introduced into each resonator, with one located at the center and the other two at the upper and the lower portions of the resonator, as shown in Figure 1c. To be consistent, we refer to this slotted system as the "3 slots" design, and similarly, we have "0 slots", "1 slot", and "2 slots" designs (see Figure 2 for details). To understand the generation of the quasi-BIC mode, we consider the two inverted electric dipoles (black arrows in the dash box of Figure 1b) excited in the two resonators of a unit-cell by an x-polarized plane wave. We decompose each electric dipole into two components p_x and p_y. Although p_y is dominant in each resonator, their directions are inverted in the two resonators, which results in them canceling each other out, and thus are decoupled from the radiative continuum. When the tilt angle is small, the overall radiative loss is suppressed significantly, and only the p_x component is found in the reflected light field (see Figure S1 for details). Hence, a narrow reflectance peak as well as a high field enhancement can be obtained.

The first noticeable improvement of adding slots is the increased Q. Compared to the "0 slot" design, a dramatic increase in Q by as much as a factor of 2 appears when at least one slot is added into the original resonator. The Q continues to increase for the "2 slots" and "3 slots" cases, as depicted in Table 1. In those simulations, we used a tilt angle (θ) of $\pm 20^\circ$

Table 1. Resonance Response Comparison for "0 Slots" to "3 Slots"

	0 slots	1 slot	2 slots	3 slots
Q	185	367	463	613
max[$\lvert E\rvert/\lvert E_0\rvert$] at apex	36.5	44.0	48.0	53.1
[$\lvert E\rvert/\lvert E_0\rvert$] at slot center	NA[a]	34.2	28.6, 35.8	32.8, 39.2, 32.8
average surface enhancement δ	139.8	296.9	364.6	453.9

[a]NA, not applicable.

so that they could be directly benchmarked with ref 25. We find that the simulated Q of the "0 slot" design is comparable to the reported value (~200), while our slotted design exhibits significantly improved Qs.

In addition to the spectral properties, the field enhancement of quasi-BIC modes is also substantially improved by introducing slots. While the highest field enhancement of all designs is located close to the resonator apex due to the collective resonance,[25,44,45] the field enhancement values are different: the field enhancement at the apex increases with respect to the number of introduced slots, as shown in Figure 2b−e. We attribute this to the fact that the Q increases with additional slots, and thus, the increased local density of states leads to the higher local electric fields.[46] Besides the field confinement at the apex, the slot effect confines and enhances the electric field in the slots due to the high relative permittivity of silicon. The electric field vectors in slots are oriented along the long axis of the ellipse, denoting the resonances as electric dipoles. To better understand the mechanism of the quasi-BIC mode, we performed the multipole decomposition analysis of the "1 slot" design following referenced procedures.[38,47−50] The multipole decomposition shows that only the electric dipole component has contributions before and after adding the slot (Figures 2f and S8), validating that the nature of the modes is maintained. The increased field enhancement of the slotted design is also manifested in the larger electric dipole component.

Quantitatively, we compare the field enhancements of different slotted designs by extracting $\lvert E\rvert/\lvert E_0\rvert$ at the apex and the slot center. It can be found that by simply adding three slots, the maximum electric field enhancement at the apex is increased up to 53.1, i.e., 2820-times for the intensity enhancement, which is 2.1-times the intensity enhancement of the original "0 slots" design, as shown in Table 1. Thus, introducing slots provides a simple way to enhance the local field and Q, which is of vital importance for lasing. Furthermore, the added slots provide extra "hot spots" for

https://doi.org/10.1021/acs.nanolett.2c01919
Nano Lett. 2022, 22, 8060−8067

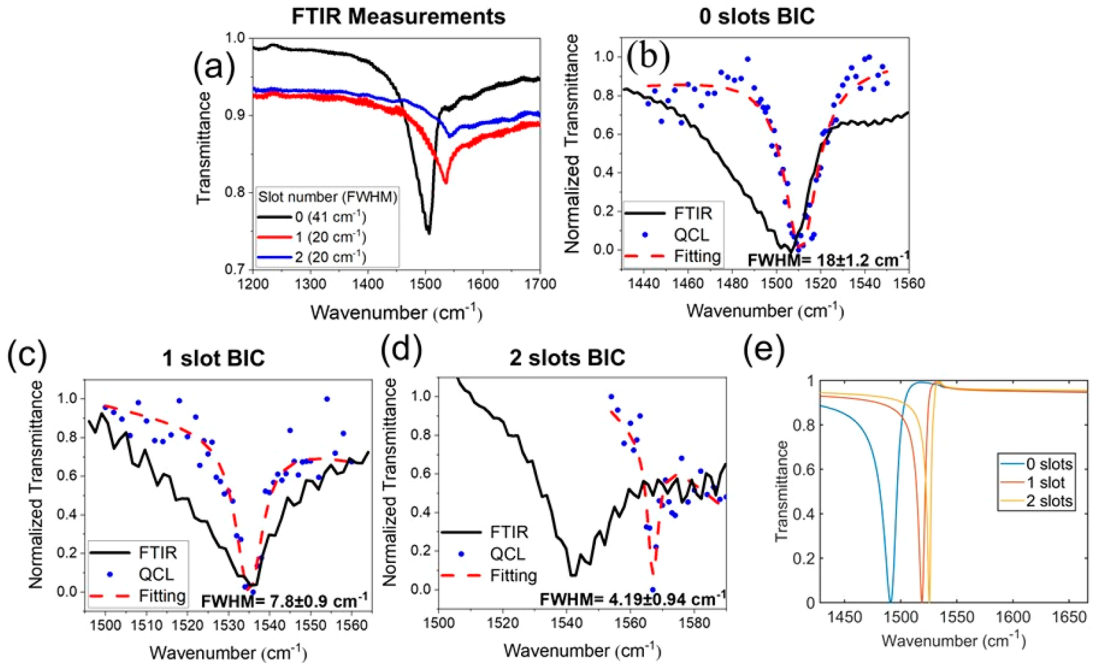

Figure 3. Spectroscopy measurements on fabricated samples. (a) FTIR transmission measurements for "0 slots" to "2 slots" samples. The measured transmission is defined as $\text{Power}_{\text{metasurface}}/\text{Power}_{\text{MgF}_2\text{substrate}}$. (b–d) Normalized transmission of "0 slots" to "2 slots" samples measured with the home-built laser spectroscopy, respectively. The FTIR measurements in the frequency range of interest extracted from panel a are normalized and plotted in corresponding figures as a comparison. The curve fittings are all performed with Lorentz fitting by commercially available software Origin 2021b. (e) Simulated spectra for "0 slots" to "2 slots" designs.

strong interaction between fields and particles or molecules as these slots all have a significant field enhancement. In contrast, the only effective regions of the "0 slots" resonator original design are at the apexes, with the central part of the resonator having almost no accessible field enhancement. The electric field in the middle slot of the "3 slots" design is even comparable to that at the ellipse apex of the "0 slots" design. Therefore, these extra "hot spots" offer significant potential for applications such as optical trapping, biosensing, and emission enhancement. For example, considering an application of sensing protein molecules,[51] the inner walls of the three slots increase the total surface area where protein molecules can bind within a high field localization region. To quantify this improvement, we define the average surface enhancement δ as the integral of the electric field intensity enhancement over the total accessible surface area normalized by the area of one unit-cell. δ is expressed as

$$\delta = \frac{1}{P_x P_y} \iint_A (|E|/|E_0|)^2 \, da \tag{1}$$

where A is the surface area of an ellipse plus that of the inner walls of the slots for slotted designs. The "3 slots" design increases δ by a factor of 2.25 compared with the original "0 slots" design, as shown in Table 1. This increased average surface enhancement is promising for applications requiring spatial overlap between the local field and the target. As an example, we illustrate how it facilitates biomaterial sensing application, e.g., monolayer protein detection. Following the discussions by Aurelian John-Herpin et al.,[52] we simulated an ideal situation where the (slotted) metasurface is coated by a conformal protein monolayer. Detailed discussions are shown in the SI, section S4.

To validate our design principle, we fabricated large-scale (0.5 mm by 0.5 mm array) patterns and performed spectroscopy measurements with representative SEM shown in Figure 1e. To be compatible with our spectral resolution, we tune the geometry parameters with a tilt angle of ±35° for "0 slots" to "2 slots" designs, with the simulated transmittance spectra shown in Figure 3e. More fabrication details are provided in the SI, section S2. We first measured the samples with FTIR (Figure 3a), and the experimental results confirm that spectra of the slotted designs have a narrower line width and shift to a larger wavenumber compared with the "0 slots" structure. However, the broadband light source (a glowbar lamp) used in FTIR caused unavoidable beam divergence: the spectral responses acquired are an integration of responses at different incident angles. As reported in ref 27, the resonant response of this zigzag quasi-BIC metasurface is highly sensitive to the incident angle. Therefore, the beam divergence broadens and damps the resonance, and the slotted designs are more sensitive to it, damping the resonances more severely (see the SI, section S3 for more discussions). Although the FTIR results do not provide quantitative line width information, they still qualitatively validate our numerical simulations that adding slots would increase the Q and shift the resonance to larger wavenumbers (Figure 3e).

To obtain the spectral response of samples without the influence of such large beam divergence, we performed transmission laser-based spectroscopy with a tunable quantum cascade laser (QCL). The experimental setup is shown in Figure 1d. More measurement details are provided in the SI, section S3. The beam divergence of the QCL is only 2 mrad, which can be safely neglected, allowing us to determine the line shape of the quasi-BIC resonances more precisely. Indeed, we find that the full-width at half-maximum (fwhm) of all samples measured with the QCL is smaller than the values

https://doi.org/10.1021/acs.nanolett.2c01919
Nano Lett. 2022, 22, 8060−8067

Table 2. Comparison between Measurements and Simulations[a]

	resonance frequency (cm^{-1})		resonance fwhm (cm^{-1})		Q		max[|E|/|E_0|] at apex
number of slots	sim.	exp.	sim.	exp.	sim.	exp.	sim.
0	1488	1511 (0.3)	16	18 (1.2)	93.3	84 (5.6)	19.5
1	1513	1535 (0.2)	9	7.8 (0.9)	170	197 (23)	24.1
2	1519	1567 (0.3)	7	4.2 (0.9)	219	373 (80)	27.9

[a]Standard deviation of the resonance frequency and fwhm are extracted from Lorentz fitting, which is included in the parentheses, and the corresponding errors of the Q are calculated by the error propagation equation.

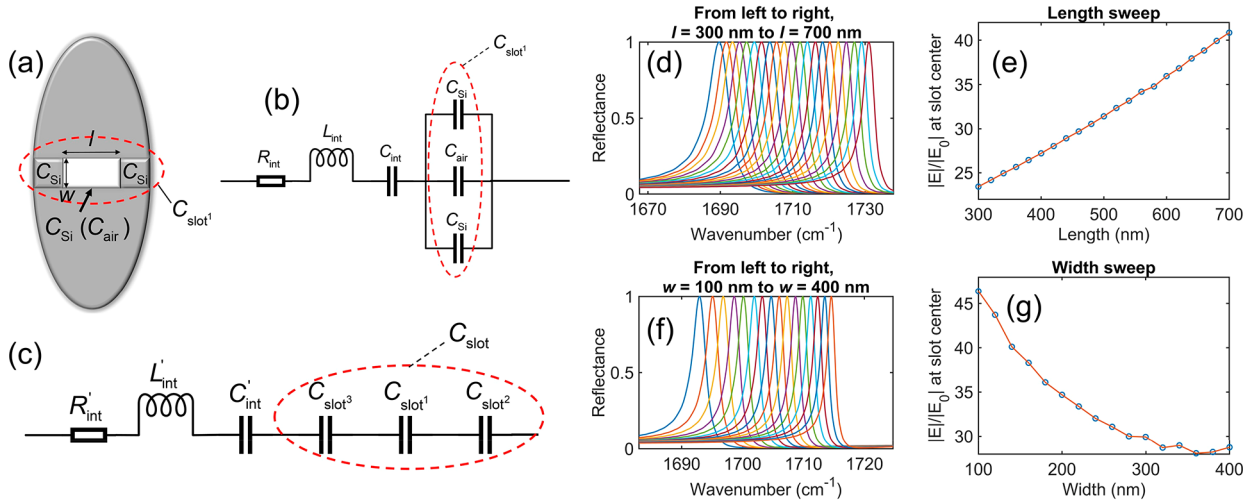

Figure 4. Equivalent circuit models and size-dependent resonant responses of the "1 slot" design. (a) Load nanocapacitance before and after introducing a slot to the resonator. Here w and l are the width and length of the air slot, respectively. (b) Equivalent circuit model for the "1 slot" design. (c) Equivalent circuit model for multislots design. Here letters R, L, and C stand for resistance, inductance, and capacitance, respectively, and "int" means intrinsic. (d) Spectra with different slot lengths l and the fixed width w = 180 nm. The solid lines correspond to l = 300 nm to l = 700 nm from left to right. (e) Field enhancement at the center of the slot with respect to different slot lengths in panel d. (f) Spectra with different slot width w and the fixed length l = 600 nm. The solid lines correspond to w = 100 nm to w = 400 nm from left to right. (g) Field enhancement at the center of the slot with respect to different slot widths in panel f.

observed via FTIR measurements. Note that the trend of the QCL measurements remains consistent with the FTIR measurements, and the slotted designs exhibit higher Qs than the "0 slots" designs. More specifically, the Q of the "0 slots" structure is determined to be 84 with a fwhm of 18 cm^{-1} (Figure 3b), which agrees well with our numerical simulation (Q of 93 and fwhm of 16 cm^{-1}). The Q of the "1 slot" sample is increased from 84 to 197 (Figure 3c). Furthermore, the Q of the "2 slots" design is even higher (373 ± 80), and the line width (4.2 ± 0.9 cm^{-1}) is approaching our instrumental limits (~1 cm^{-1}), as shown in Figure 3d. The extracted resonance properties are tabulated in Table 2. We assume the relatively large difference between the QCL measurement and the numerical simulation for the "2 slots" sample comes from the sample loading process and/or fabrication imperfections. Therefore, the laser spectroscopy measurements as well as the FTIR measurements validate that the slotted designs manifest narrower line widths and shift the resonances to larger wavenumbers. Moreover, we anticipate comparable field enhancements in the actual samples considering the good agreements between simulations and experiments.

To understand and predict the spectral response of the slotted design, we implement an effective impedance model by regarding each silicon resonator as a nanoantenna based on the optical nanoantenna theory.[53−59] For simplicity, we assume that the dominant contribution of the near-field electric polarization comes from the electric dipole moment. The resonator only has radiative loss and is positioned in a homogeneous background (i.e., air in this work). When only considering the radiative loss, generally a single dipolar nanoantenna can be approximated with a series RLC circuit, associated with the intrinsic impedance of the system expressed as[25]

$$Z_{\text{int}} = R_{\text{int}} - jX_{\text{int}} = R_{\text{int}} - j\omega L_{\text{int}} - \frac{1}{j\omega C_{\text{int}}} \tag{2}$$

where j is the imaginary unit, and R_{int} is the intrinsic resistance and is contributed by the radiative loss. According to ref 53, a dipolar nanoantenna with one loaded gap at the center can act as the series combination of the intrinsic impedance and the load impedance when excited by an external plane wave with the electric field parallel to the nanodipole axis. For positive values of the real part of permittivities for dielectric materials, the optical impedance is capacitive. Since the silicon resonator is approximated as a dipole antenna with the direction of the main dipole moment along the long axis of the ellipse, it is reasonable to regard the original "0 slots" resonator as a nanoantenna with a gap loaded with silicon (ε_r = 10.30), as shown in Figure 4a. The load nanocapacitance is expressed as[54,57]

$$C^0_{\text{slot}^1} = \varepsilon_0 \varepsilon_r Hb/w \tag{3}$$

When introducing a slot (i.e., the "1 slot" resonator), part of the gap is unloaded (i.e., filled with air) and then the gap can be equivalent to a parallel connection of three capacitors, also

https://doi.org/10.1021/acs.nanolett.2c01919
Nano Lett. 2022, 22, 8060−8067

seen in Figure 4a. The equivalent circuit model for the "1 slot" design is sketched in Figure 4b, and the load nanocapacitance is now given by

$$C_{\text{slot}^1} = C_{\text{Si}} + C_{\text{air}} + C_{\text{Si}} = \frac{\varepsilon_0 H}{w}[\varepsilon_r b - (\varepsilon_r - 1)l] \tag{4}$$

When $l = 0$ (i.e., the air slot is not introduced), $C_{\text{slot}^1} = C^0_{\text{slot}^1}$. The resonance peak is achieved when the optical frequency ω equals ω_0, where ω_0 is the open-circuit resonance frequency expressed as[55]

$$\omega_0 = \frac{1}{X_{\text{int}} C_{\text{slot}^1}} \tag{5}$$

When the slot length l is not 0, C_{slot^1} is always smaller than the nanocapacitance of the "0 slots" design $C^0_{\text{slot}^1}$. The resonance frequency ω_0 thus increases, indicating the reflectance peak shifts to a larger wavenumber. For this series RLC circuit, the Q is defined as $Q = R_{\text{int}}^{-1}\sqrt{L_{\text{int}}/C_{\text{system}}} \propto \sqrt{1/C_{\text{system}}}$. Here, C_{system} is the series connection of C_{int} and C_{slot^1} expressed as

$$C_{\text{system}} = (1/C_{\text{int}} + 1/C_{\text{slot}^1})^{-1} \tag{6}$$

With a decreased C_{slot^1} by introducing an air slot, the Q increases, explaining the narrower line width of the reflectance spectrum of the "1 slot" design. For multislot designs (i.e., "2 slots" and "3 slots"), the equivalent circuit model for the load is a series connection of capacitors (see Figure 4c) with part of the load material changing from silicon to air by introducing air slots, leading to the decrease of the load nanocapacitance C_{slot}. Therefore, the reflectance peaks shift to larger wavenumbers, and the Qs are higher when we introduce more slots, as observed in Figure 2a.

Next, we investigate the impacts of the slot size on both spectra and local field responses by exemplifying the "1 slot" design with the effective impedance model. The continuous evolution of the spectra and the electric field enhancement at the center of the slot are shown in Figure 4. When increasing the slot length l with a fixed width w, the reflectance peak shifts to a larger wavenumber while the Q slightly increases as well, as shown in Figure 4d. When we increase the slot width w with a fixed length l, the reflectance peak shifts to a larger wavenumber while the Q still slightly increases, as shown in Figure 4f. Both behaviors are well predicted by the effective impedance model. According to eq 4, a wider gap w and/or a longer length l would decrease C_{slot^1}, leading to a higher resonance frequency and a larger Q. Notably, length and width play different roles in the field enhancement at the slot, as shown in Figure 4e and g. A longer slot induces a higher Q, thus having a higher field enhancement, while a wider slot has a lower field enhancement at the center of the slot, mainly attributed to the continuity of the normal component of the electric displacement field. We note that the electric field at the apex of the resonator arises when the Q increases, i.e., when w or l increases.

In summary, we have proposed and experimentally demonstrated a new mechanism for tuning the resonant response of a quasi-BIC-governed all-dielectric metasurface composed of elliptical silicon resonators arranged in a zigzag array by symmetrically introducing slots into each resonator. We show that by introducing slots, the quality factor and electric field intensity can be enhanced by as much as 3.3-times and 2.1-times compared with the original structure without slots, while the quasi-BIC mode is still preserved. Moreover, the enhanced and spatially confined field in the slots provides extra electromagnetic "hot spots" for field-target interaction. By implementing an effective impedance model based on the optical nanoantenna theory, we analytically explain the spectral responses of the slotted metasurface. We envision that these results may find many applications in low-threshold lasing, sensing, biomolecular trapping, nonlinear optics, and engineering spontaneous emission. Our presented design methodology is also readily extendable to other dipole-based single and periodic nanostructures.

■ ASSOCIATED CONTENT

Supporting Information

The Supporting Information is available free of charge at https://pubs.acs.org/doi/10.1021/acs.nanolett.2c01919.

Numerical simulation details; metasurface fabrication process; spectral measurements details; additional discussions on influence of angular spread over BIC measurements; theoretical discussions on application of protein detection; details on multipole decomposition (PDF)

■ AUTHOR INFORMATION

Corresponding Author

Justus C. Ndukaife − *Department of Electrical and Computer Engineering, Department of Mechanical Engineering, and Interdisciplinary Materials Science, Vanderbilt University, Nashville, Tennessee 37235, United States; Vanderbilt Institute of Nanoscale Science and Engineering, Vanderbilt University, Nashville, Tennessee 37235, United States;* orcid.org/0000-0002-8524-0657; Email: justus.ndukaife@vanderbilt.edu

Authors

Sen Yang − *Interdisciplinary Materials Science, Vanderbilt University, Nashville, Tennessee 37235, United States; Vanderbilt Institute of Nanoscale Science and Engineering, Vanderbilt University, Nashville, Tennessee 37235, United States;* orcid.org/0000-0002-0056-3052

Mingze He − *Department of Mechanical Engineering, Vanderbilt University, Nashville, Tennessee 37235, United States; Vanderbilt Institute of Nanoscale Science and Engineering, Vanderbilt University, Nashville, Tennessee 37235, United States;* orcid.org/0000-0001-8773-1268

Chuchuan Hong − *Department of Electrical and Computer Engineering, Vanderbilt University, Nashville, Tennessee 37235, United States; Vanderbilt Institute of Nanoscale Science and Engineering, Vanderbilt University, Nashville, Tennessee 37235, United States;* orcid.org/0000-0002-1329-9385

Joshua D. Caldwell − *Department of Mechanical Engineering and Interdisciplinary Materials Science, Vanderbilt University, Nashville, Tennessee 37235, United States; Vanderbilt Institute of Nanoscale Science and Engineering, Vanderbilt University, Nashville, Tennessee 37235, United States;* orcid.org/0000-0003-0374-2168

Complete contact information is available at: https://pubs.acs.org/10.1021/acs.nanolett.2c01919

https://doi.org/10.1021/acs.nanolett.2c01919
Nano Lett. 2022, 22, 8060−8067

Author Contributions

J.C.N. conceived and guided the project. S.Y. designed the slotted quasi-BIC metasurface. S.Y. performed the electromagnetic simulations, built the effective impedance model, and fabricated the samples. M.H. designed and conducted the spectral measurements. C.H. did the multipole decomposition analysis and contributed to the EM simulations and the sample fabrication. J.D.C. guided the spectral measurement experiments.

Author Contributions

[¶]S.Y. and M.H. contributed equally to this work.

Notes

The authors declare no competing financial interest.

■ ACKNOWLEDGMENTS

S.Y., C.H., and J.C.N. acknowledge financial support from the National Science Foundation (NSF ECCS-1933109) and NSF CAREER Award (NSF ECCS 2143836). Fabrication of the quasi-BIC metasurfaces was conducted at the Vanderbilt Institute of Nanoscale Science and Engineering. J.D.C. acknowledges support from NSF No. 2128240, while M.H. was supported by the Office of Naval Research under Grant No. N00014-22-1-2035.

■ REFERENCES

(1) Novotny, L.; Hecht, B.*Principles of Nano-Optics*; Cambridge University Press, 2012; pp 1−564. DOI: 10.1017/CBO9780511794193.

(2) Khurgin, J. B.; Boltasseva, A. Reflecting upon the Losses in Plasmonics and Metamaterials. *MRS Bull.* **2012**, *37* (8), 768−779.

(3) Khurgin, J. B.; Sun, G. Scaling of Losses with Size and Wavelength in Nanoplasmonics and Metamaterials. *Appl. Phys. Lett.* **2011**, *99* (21), 211106.

(4) Altug, H.; Oh, S. H.; Maier, S. A.; Homola, J. Advances and Applications of Nanophotonic Biosensors. *Nature Nanotechnology* **2022**, *17* (1), 5−16.

(5) Hakala, T. K.; Rekola, H. T.; Väkeväinen, A. I.; Martikainen, J. P.; Nečada, M.; Moilanen, A. J.; Törmä, P. Lasing in Dark and Bright Modes of a Finite-Sized Plasmonic Lattice. *Nature Communications* **2017**, *8* (1), 1−7.

(6) Wu, C.; Khanikaev, A. B.; Adato, R.; Arju, N.; Yanik, A. A.; Altug, H.; Shvets, G. Fano-Resonant Asymmetric Metamaterials for Ultrasensitive Spectroscopy and Identification of Molecular Monolayers. *Nature Materials* **2012**, *11* (1), 69−75.

(7) Adato, R.; Yanik, A. A.; Amsden, J. J.; Kaplan, D. L.; Omenetto, F. G.; Hong, M. K.; Erramilli, S.; Altug, H. Ultra-Sensitive Vibrational Spectroscopy of Protein Monolayers with Plasmonic Nanoantenna Arrays. *Proc. Natl. Acad. Sci. U. S. A.* **2009**, *106* (46), 19227−19232.

(8) Luk'Yanchuk, B.; Zheludev, N. I.; Maier, S. A.; Halas, N. J.; Nordlander, P.; Giessen, H.; Chong, C. T. The Fano Resonance in Plasmonic Nanostructures and Metamaterials. *Nat. Mater.* **2010**, *9* (9), 707−715.

(9) Deng, S.; Li, R.; Park, J.-E.; Guan, J.; Choo, P.; Hu, J.; Smeets, P. J. M.; Odom, T. W. Ultranarrow Plasmon Resonances from Annealed Nanoparticle Lattices. *Proc. Natl. Acad. Sci. U. S. A.* **2020**, *117* (38), 23380−23384.

(10) Le-Van, Q.; Zoethout, E.; Geluk, E. J.; Ramezani, M.; Berghuis, M.; Gómez Rivas, J. Enhanced Quality Factors of Surface Lattice Resonances in Plasmonic Arrays of Nanoparticles. *Advanced Optical Materials* **2019**, *7* (6), 1801451.

(11) Bin-Alam, M. S.; Reshef, O.; Mamchur, Y.; Alam, M. Z.; Carlow, G.; Upham, J.; Sullivan, B. T.; Ménard, J. M.; Huttunen, M. J.; Boyd, R. W.; Dolgaleva, K. Ultra-High-Q Resonances in Plasmonic Metasurfaces. *Nat. Commun.* **2021**, *12* (1), 974 DOI: 10.1038/s41467-021-21196-2.

(12) Baffou, G.; Quidant, R. Thermo-Plasmonics: Using Metallic Nanostructures as Nano-Sources of Heat. *Laser and Photonics Reviews* **2013**, *7* (2), 171−187, DOI: 10.1002/lpor.201200003.

(13) Jahani, S.; Jacob, Z. All-Dielectric Metamaterials. *Nature Nanotechnology* **2016**, *11* (1), 23−36.

(14) Koshelev, K.; Kivshar, Y. Dielectric Resonant Metaphotonics. *ACS Photonics* **2021**, *8* (1), 102−112, DOI: 10.1021/acsphotonics.0c01315.

(15) Yang, Y.; Kravchenko, I. I.; Briggs, D. P.; Valentine, J. All-Dielectric Metasurface Analogue of Electromagnetically Induced Transparency. *Nature Communications* **2014**, *5* (1), 1−7.

(16) von Neumann, J.; Wigner, E. Über Merkwürdige Diskrete Eigenwerte. *Phys. Z.* **1929**, *30*, 465−467.

(17) Hsu, C. W.; Zhen, B.; Stone, A. D.; Joannopoulos, J. D.; Soljacic, M. Bound States in the Continuum. *Nature Reviews Materials* **2016**, *1* (9), 1−13.

(18) Lee, J.; Zhen, B.; Chua, S. L.; Qiu, W.; Joannopoulos, J. D.; Soljačić, M.; Shapira, O. Observation and Differentiation of Unique High-Q Optical Resonances near Zero Wave Vector in Macroscopic Photonic Crystal Slabs. *Phys. Rev. Lett.* **2012**, *109* (6), 067401 DOI: 10.1103/PhysRevLett.109.067401.

(19) Hsu, C. W.; Zhen, B.; Lee, J.; Chua, S. L.; Johnson, S. G.; Joannopoulos, J. D.; Soljačić, M. Observation of Trapped Light within the Radiation Continuum. *Nature* **2013**, *499* (7457), 188−191.

(20) Plotnik, Y.; Peleg, O.; Dreisow, F.; Heinrich, M.; Nolte, S.; Szameit, A.; Segev, M. Experimental Observation of Optical Bound States in the Continuum. *Phys. Rev. Lett.* **2011**, *107* (18), 183901 DOI: 10.1103/PhysRevLett.107.183901.

(21) Chen, Z.; Yin, X.; Jin, J.; Zheng, Z.; Zhang, Z.; Wang, F.; He, L.; Zhen, B.; Peng, C. Observation of Miniaturized Bound States in the Continuum with Ultra-High Quality Factors. *Science Bulletin* **2022**, *67* (4), 359−366.

(22) Kodigala, A.; Lepetit, T.; Gu, Q.; Bahari, B.; Fainman, Y.; Kanté, B. Lasing Action from Photonic Bound States in Continuum. *Nature* **2017**, *541* (7636), 196−199.

(23) Hwang, M. S.; Lee, H. C.; Kim, K. H.; Jeong, K. Y.; Kwon, S. H.; Koshelev, K.; Kivshar, Y.; Park, H. G. Ultralow-Threshold Laser Using Super-Bound States in the Continuum. *Nat. Commun.* **2021**, *12* (1), 4135 DOI: 10.1038/s41467-021-24502-0.

(24) Huang, C.; Zhang, C.; Xiao, S.; Wang, Y.; Fan, Y.; Liu, Y.; Zhang, N.; Qu, G.; Ji, H.; Han, J.; Ge, L.; Kivshar, Y.; Song, Q. Ultrafast Control of Vortex Microlasers. *Science* **2020**, *367* (6481), 1018−1021.

(25) Choi, D.-Y.; Kivshar, Y. S.; Neshev, D. N.; Liu, M.; Altug, H.; Tittl, A.; Yesilkoy, F.; Leitis, A. Imaging-Based Molecular Barcoding with Pixelated Dielectric Metasurfaces. *Science* **2018**, *360* (6393), 1105−1109.

(26) Yesilkoy, F.; Arvelo, E. R.; Jahani, Y.; Liu, M.; Tittl, A.; Cevher, V.; Kivshar, Y.; Altug, H.Ultrasensitive Hyperspectral Imaging and Biodetection Enabled by Dielectric Metasurfaces. *Nature Photonics*; Nature Publishing Group, 2019; pp 390−396. DOI: 10.1038/s41566-019-0394-6.

(27) Leitis, A.; Tittl, A.; Liu, M.; Lee, B. H.; Gu, M. B.; Kivshar, Y. S.; Altug, H. Angle-Multiplexed All-Dielectric Metasurfaces for Broadband Molecular Fingerprint Retrieval. *Science Advances* **2019**, *5* (5), No. eaaw2871.

(28) Yang, S.; Hong, C.; Jiang, Y.; Ndukaife, J. C. Nanoparticle Trapping in a Quasi-BIC System. *ACS Photonics* **2021**, *8* (7), 1961−1971.

(29) Hong, C.; Yang, S.; Kravchenko, I. I.; Ndukaife, J. C. Electrothermoplasmonic Trapping and Dynamic Manipulation of Single Colloidal Nanodiamond. *Nano Lett.* **2021**, *21* (12), 4921−4927.

(30) Koshelev, K.; Tang, Y.; Li, K.; Choi, D. Y.; Li, G.; Kivshar, Y. Nonlinear Metasurfaces Governed by Bound States in the Continuum. *ACS Photonics* **2019**, *6* (7), 1639−1644.

(31) Liu, Z.; Xu, Y.; Lin, Y.; Xiang, J.; Feng, T.; Cao, Q.; Li, J.; Lan, S.; Liu, J. High- Q Quasibound States in the Continuum for

Nonlinear Metasurfaces. *Phys. Rev. Lett.* **2019**, *123*, 253901 DOI: 10.1103/PhysRevLett.123.253901.
(32) Carletti, L.; Koshelev, K.; de Angelis, C.; Kivshar, Y. Giant Nonlinear Response at the Nanoscale Driven by Bound States in the Continuum. *Phys. Rev. Lett.* **2018**, *121* (3), 33903.
(33) Koshelev, K.; Kruk, S.; Melik-Gaykazyan, E.; Choi, J.-H.; Bogdanov, A.; Park, H.-G.; Kivshar, Y. Subwavelength Dielectric Resonators for Nonlinear Nanophotonics. *Science* **2020**, *367* (6475), 288−292.
(34) Koshelev, K.; Bogdanov, A.; Kivshar, Y. Meta-Optics and Bound States in the Continuum. *Science Bulletin* **2019**, *64* (12), 836−842.
(35) Koshelev, K.; Lepeshov, S.; Liu, M.; Bogdanov, A.; Kivshar, Y. Asymmetric Metasurfaces with High- Q Resonances Governed by Bound States in the Continuum. *Phys. Rev. Lett.* **2018**, *121*, 193903 DOI: 10.1103/PhysRevLett.121.193903.
(36) Han, S.; Cong, L.; Srivastava, Y. K.; Qiang, B.; Rybin, M. v.; Kumar, A.; Jain, R.; Lim, W. X.; Achanta, V. G.; Prabhu, S. S.; Wang, Q. J.; Kivshar, Y. S.; Singh, R. All-Dielectric Active Terahertz Photonics Driven by Bound States in the Continuum. *Adv. Mater.* **2019**, *31* (37), 1901921.
(37) Bogdanov, A. A.; Koshelev, K. L.; Kapitanova, P. v.; Rybin, M. v.; Gladyshev, S. A.; Sadrieva, Z. F.; Samusev, K. B.; Kivshar, Y. S.; Limonov, M. F. Bound States in the Continuum and Fano Resonances in the Strong Mode Coupling Regime. *Advanced Photonics* **2019**, *1* (1), 016001.
(38) Yang, Y.; Zenin, V. A.; Bozhevolnyi, S. I. Anapole-Assisted Strong Field Enhancement in Individual All-Dielectric Nanostructures. *ACS Photonics* **2018**, *5* (5), 1960−1966.
(39) Yang, A. H. J.; Moore, S. D.; Schmidt, B. S.; Klug, M.; Lipson, M.; Erickson, D. Optical Manipulation of Nanoparticles and Biomolecules in Sub-Wavelength Slot Waveguides. *Nature* **2009**, *457* (7225), 71−75.
(40) Moretti, G. Q.; Cortés, E.; Maier, S. A.; Bragas, A. v.; Grinblat, G. Engineering Gallium Phosphide Nanostructures for Efficient Nonlinear Photonics and Enhanced Spectroscopies. *Nanophotonics* **2021**, *10* (17), 4261−4271.
(41) Fang, C.; Yang, Q.; Yuan, Q.; Gu, L.; Gan, X.; Shao, Y.; Liu, Y.; Han, G.; Hao, Y. Efficient Second-Harmonic Generation from Silicon Slotted Nanocubes with Bound States in the Continuum. *Laser and Photonics Reviews* **2022**, *16*, 2100498.
(42) Han, Z.; Ding, F.; Cai, Y.; Levy, U. Significantly Enhanced Second-Harmonic Generations with All-Dielectric Antenna Array Working in the Quasi-Bound States in the Continuum and Excited by Linearly Polarized Plane Waves. *Nanophotonics* **2021**, *10* (3), 1189−1196.
(43) Ahmadivand, A.; Gerislioglu, B. Photonic and Plasmonic Metasensors. *Laser and Photonics Reviews* **2022**, *16* (2), 2100328.
(44) Liu, M.; Choi, D. Y. Extreme Huygens' Metasurfaces Based on Quasi-Bound States in the Continuum. *Nano Lett.* **2018**, *18* (12), 8062−8069.
(45) Liu, M.; Powell, D. A.; Guo, R.; Shadrivov, I. V.; Kivshar M Liu, Y. S. Polarization-Induced Chirality in Metamaterials via Optomechanical Interaction. *Advanced Optical Materials* **2017**, *5* (16), 1600760.
(46) Shahbazyan, T. v. Local Density of States for Nanoplasmonics. *Phys. Rev. Lett.* **2016**, *117*, 207401 DOI: 10.1103/PhysRevLett.117.207401.
(47) Yang, Y.; Miroshnichenko, A. E.; Kostinski, S. v.; Odit, M.; Kapitanova, P.; Qiu, M.; Kivshar, Y. S. Multimode Directionality in All-Dielectric Metasurfaces. *Phys. Rev. B* **2017**, *95* (16), 165426.
(48) Evlyukhin, A. B.; Fischer, T.; Reinhardt, C.; Chichkov, B. N. Optical Theorem and Multipole Scattering of Light by Arbitrarily Shaped Nanoparticles. *Phys. Rev. B* **2016**, *94* (20), 205434.
(49) Grahn, P.; Shevchenko, A.; Kaivola, M. Electromagnetic Multipole Theory for Optical Nanomaterials. *New J. Phys.* **2012**, *14* (9), 093033.
(50) Evlyukhin, A. B.; Reinhardt, C.; Chichkov, B. N. Multipole Decomposition in Discrete Dipole Approximation. *AIP Conf. Proc.* **2012**, *1475* (1), 125.
(51) Yoo, D.; Mohr, D. A.; Vidal-Codina, F.; John-Herpin, A.; Jo, M.; Kim, S.; Matson, J.; Caldwell, J. D.; Jeon, H.; Nguyen, N. C.; Martin-Moreno, L.; Peraire, J.; Altug, H.; Oh, S. H. High-Contrast Infrared Absorption Spectroscopy via Mass-Produced Coaxial Zero-Mode Resonators with Sub-10 Nm Gaps. *Nano Lett.* **2018**, *18* (3), 1930−1936.
(52) John-Herpin, A.; Tittl, A.; Altug, H. Quantifying the Limits of Detection of Surface-Enhanced Infrared Spectroscopy with Grating Order-Coupled Nanogap Antennas. *ACS Photonics* **2018**, *5* (10), 4117−4124.
(53) Alù, A.; Engheta, N. Wireless at the Nanoscale: Optical Interconnects Using Matched Nanoantennas. *Phys. Rev. Lett.* **2010**, *104* (21), 213902.
(54) Al, A.; Engheta, N. Tuning the Scattering Response of Optical Nanoantennas with Nanocircuit Loads. *Nature Photonics* **2008**, *2* (5), 307−310.
(55) Salandrino, A.; Alù, A.; Engheta, N. Parallel, Series, and Intermediate Interconnections of Optical Nanocircuit Elements. 2. Nanocircuit and Physical Interpretation. *JOSA B* **2007**, *24* (12), 3014−3022, DOI: 10.1364/JOSAB.24.003014.
(56) Alù, A.; Engheta, N. Input Impedance, Nanocircuit Loading, and Radiation Tuning of Optical Nanoantennas. *Phys. Rev. Lett.* **2008**, *101* (4), 043901.
(57) Alù, A.; Engheta, N.; Zhao, Y.Effects of Shape and Loading of Optical Nanoantennas on Their Sensitivity and Radiation Properties. *JOSA B*2011, *28* (5), 1266−1274. DOI: 10.1364/JOSAB.28.001266.
(58) Engheta, N.; Salandrino, A.; Alù, A. Circuit Elements at Optical Frequencies: Nanoinductors, Nanocapacitors, and Nanoresistors. *Phys. Rev. Lett.* **2005**, *95* (9), 095504.
(59) Agio, M.; Alù, A.*Optical Antennas*; Cambridge University Press, 2013; pp 1−455. DOI: 10.1017/CBO9781139013475.

https://doi.org/10.1021/acs.nanolett.2c01919
Nano Lett. 2022, 22, 8060−8067